Environmental Science: Atmospheres

ROYAL SOCIETY OF CHEMISTRY

PAPER

View Article Online
View Journal

Cite this: DOI: 10.1039/d5ea00111k

Evaluating the effects of COVID-19 lockdowns on air quality across some African countries

Zizhen Han,[a] Yuqiang Zhang,*[a] Zhou Liu,[a] Kexin Zhang,[bc] Stanley Numbonui Tasheh,[d] Narcisse Tchinda Tsona,[a] Zhuyi Wang,[a] Bin Luo,[a] Likun Xue[a] and Xinfeng Wang*[a]

The COVID-19 lockdown served as a pivotal moment to analyze significant changes in air quality due to unprecedented reductions in emissions across major African countries. This study assesses the alterations in air quality, focusing on key pollutants such as CO, NO_2, O_3, SO_2 and aerosol particles during the lockdown period in 2020. Utilizing chemical reanalysis data from the state-of-the-art multi-component satellite data assimilation system at the Jet Propulsion Laboratory, quarterly anomalies were calculated for March to May (MAM) and June to August (JJA). The analysis reveals a significant decline in CO, NO_2, O_3 and nitrate aerosols across most African nations, with more pronounced decreases observed during the JJA period. However, notable discrepancies emerged: quarterly dual anomalies indicated a reduction in NO_2 and SO_2 levels in Northern Africa, while quarterly anomalies suggested an increase, indicating that containment policies affected these trends. In Southern Africa (SA), both quarters witnessed increases in SO_2 levels, likely due to relaxed restrictions and heightened energy demands. Additionally, the rise in O_3 levels in SA may be associated with the decrease in NO_2. The increase in sulfate and ammonium aerosols in Northern and Southern Africa is likely attributed to dust events and elevated residential emissions, respectively. The findings from this study highlight that air quality changes are influenced by a combination of natural and anthropogenic factors, stressing the urgent need for stricter emission standards for coal-fired plants and the promotion of clean energy initiatives throughout African countries.

Received 12th September 2025
Accepted 23rd January 2026

DOI: 10.1039/d5ea00111k

rsc.li/esatmospheres

Environmental significance

Due to the scarcity of reliable monitoring data, there are no relevant studies on the air pollutant changes in most African countries during COVID-19 lockdown periods. Our study fills this gap. Based on our analysis of these results, our study highlights key issues and directions that Africa needs to address in order to improve air quality.

1 Introduction

The strict containment policies during the outbreak of coronavirus disease 2019 (referred to as COVID-19) in 2020, such as partial or complete closure of international borders, schools, and non-essential businesses, as well as restrictions on citizen movement in some cases,[1] provided a natural experiment to investigate how the air quality will respond to potential strict control policies.[2–4] Numerous studies have investigated the air quality changes due to the lockdown measures across different regions worldwide using surface observation, air quality modelling and satellite retrievals. However, the responses to the air quality changes were highly dependent on the species and location and were not always consistent.

Many studies have shown that strict lockdown measures have led to significant improvements for certain pollutants, but no noticeable decrease for others. Take a few examples, the cities of Chongqing, Luzhou, and Chengdu in China experienced the largest decreases in nitrogen dioxide (NO_2) and sulfur dioxide (SO_2) by 62.1% and 83.8% individually from February 2020 compared with previous years (2017–2019), while carbon monoxide (CO), PM_{10}, and $PM_{2.5}$ had relatively smaller decreases, ranging from 17.9% to 30.8%. Surprisingly, O_3 concentration increased by 6.2% instead.[5] In addition, although reduced anthropogenic emissions during the lockdown period

[a]Environmental Research Institute, Shandong University, Qingdao 266237, China. E-mail: yuqiang.zhang@sdu.edu.cn; xinfengwang@sdu.edu.cn

[b]School of Environmental Science and Engineering, Shandong University, Qingdao 266237, China

[c]Shenzhen Key Laboratory of Ecological Remediation and Carbon Sequestration, Institute of Environment and Ecology, Tsinghua Shenzhen International Graduate School, Tsinghua University, Shenzhen 518055, China

[d]Department of Chemistry, Faculty of Science, The University of Bamenda, P.O. Box 39, Bambili, Bamenda, Cameroon

led to an obvious decrease in $PM_{2.5}$ across most provinces in China, unfavourable weather conditions, mainly less rainfall, lower planetary boundary layer (PBL) and wind speed, higher relative humidity (RH) and temperature, resulted in only half of its precursor's decline.[6] During the recent lockdown period in Shanghai, China from April to May 2022, both surface and column NO_2 exhibited a significant decrease. However, surface formaldehyde (HCHO) was found to increase by 13%, while O_3 concentration did not change significantly, due to the weakened titration effects from the reduction in NO.[7] As one of the cities most severely affected by the COVID-19 pandemic after Wuhan, Milan in Italy also observed a significant decrease in NO_2 during the lockdown period. However, while there was a 20% reduction in SO_2 concentration in urban areas, there was no change in SO_2 levels in suburban areas, possibly due to more closures of public places in urban areas resulting in a decrease in heating demand, but the suburban heating demand has not dropped significantly. Meanwhile, O_3 concentrations significantly increased in urban areas, which could be attributed to chemical oxidation reactions caused by increased sunlight hours and decreased NO_2 concentrations.[8] During the lockdown period, NO_2 concentrations were also found to decrease significantly in the United States,[9–11] while $PM_{2.5}$ only decreased in metropolitan areas of Northeastern and California/Nevada regions with O_3 concentrations remaining relatively stable.[12] Similar phenomena have also been found in other countries such as India,[2,13] Bangladesh,[14] Brazil,[15] Spain,[16] and EU member states.[17] Meanwhile, a few studies also investigated the impact of lockdown measures on air quality changes from a global perspective,[18–20] including assimilated high-resolution OMI and TROPOMI satellite retrievals or ground observation data which have found that although global anthropogenic NO_2 emissions decreased significantly during the lockdown periods in 2020, the decreases in $PM_{2.5}$ were smaller than that of NO_2 and even remained unchanged.[18,21,22] Additionally, due to the high local ozone production efficiency in Asia and America, there were little changes in the global tropospheric ozone burden.[19] Furthermore, Shi *et al.*[22] discovered that the decreases in NO_2 concentrations in 11 typical cities were lower than expected through deweathering machine learning techniques, indicating the importance of weather conditions in the air quality changes. However, to the best of our knowledge, few studies have been focused on the African continent mainly due to the lack of well-developed ground monitoring sites and the lack of attention and funding for the African environment.[23]

As the region with the highest exposure to $PM_{2.5}$ in the world, Africa's air pollution problem cannot be overlooked. With rapid urbanization, economic development and increasing reliance on fossil fuel combustion,[24–26] the air pollution-induced mortality burden has become the second leading cause of death in Africa.[27,28] The epidemic lockdown has also provided an "opportunity scenario" for African countries to study the effectiveness of emission reduction policies to improve air quality. Some available studies have been carried out to study the air quality changes in specific African cities or regions by utilizing sporadic monitoring station data[29] and remote sensing.[30] For example, in certain cities of Morocco, during the lockdown period, there was a significant decrease in NO_2 compared with before the lockdown, and $PM_{2.5}$ also relatively decreased.[29,31] In some cities in Nigeria, O_3 concentration increased slightly, while NO_2 concentration decreased in March but slightly increased in April. SO_2 concentration during the lockdown months (March and April) increased compared with previous years but with a lower magnitude than in January and February.[32] Using OMI retrieved data, NO_2 emissions decreased by 15% and 33% in Cairo and Alexandria in Egypt respectively, with a slight decrease of CO (approximately 5%) and an increase of ozone by about 2% compared with the years 2015–2019.[33] In Kampala, Uganda, one of EA's busiest cities, the Air Quality Index (AQI) showed a 6.6% decrease during the lockdown period (March to July) compared with the previous year.[34]

The primary objective of this study was to investigate changes in gas and aerosol pollutants during the COVID-19 lockdown periods across major African countries, specifically during March to May (referred to as MAM) and June to August (referred to as JJA). Chemical reanalysis products from a state-of-the-art multi-component satellite data assimilation system[19,35,36] were utilized, optimizing pollutant concentrations and emissions by assimilating multiple satellite observations and accounting for chemical interactions among different gases. To isolate the effects of temporal emission changes and interannual meteorological variations, two distinct methods were applied to quantify air quality changes: quarterly mean anomalies (the difference in pollutant concentration between 2020 and reference years from 2005 to 2019) and difference-in-difference (the difference between the February mean anomaly and the quarterly mean anomaly). Additionally, Pearson correlation coefficients were calculated to assess the relationship between changes in pollutant concentrations and variations in stringency indices or meteorological conditions during the MAM and JJA seasons.

2 Data and methodology

2.1 Study area

Fig. S1 illustrates the study area, encompassing the entire African continent, which includes 50 countries situated between 40°S and 40°N latitude and 20°W and 40°E longitude. Certain islands, such as Cabo Verde, São Tomé and Príncipe, Comoros, Mauritius, Mayotte, Réunion, Seychelles, and Saint Helena are excluded from this coverage. Additionally, the studied African countries were categorized into several regions: Northern Africa (NA), Central Africa (CA), Western Africa (WA), Eastern Africa (EA), and Southern Africa (SA), as defined by the United Nations (see Fig. S1).

2.2 Government restrictions in Africa

Since March 2020, African countries have implemented different restrictive policies in response to the COVID-19 pandemic. We obtained the indicator of the lockdown stringency measures developed by Hale *et al.*[37] to quantify the containment intensity in African countries. The index, which ranges from 0 to 100 (Fig. S2), tracks the multiple measures and

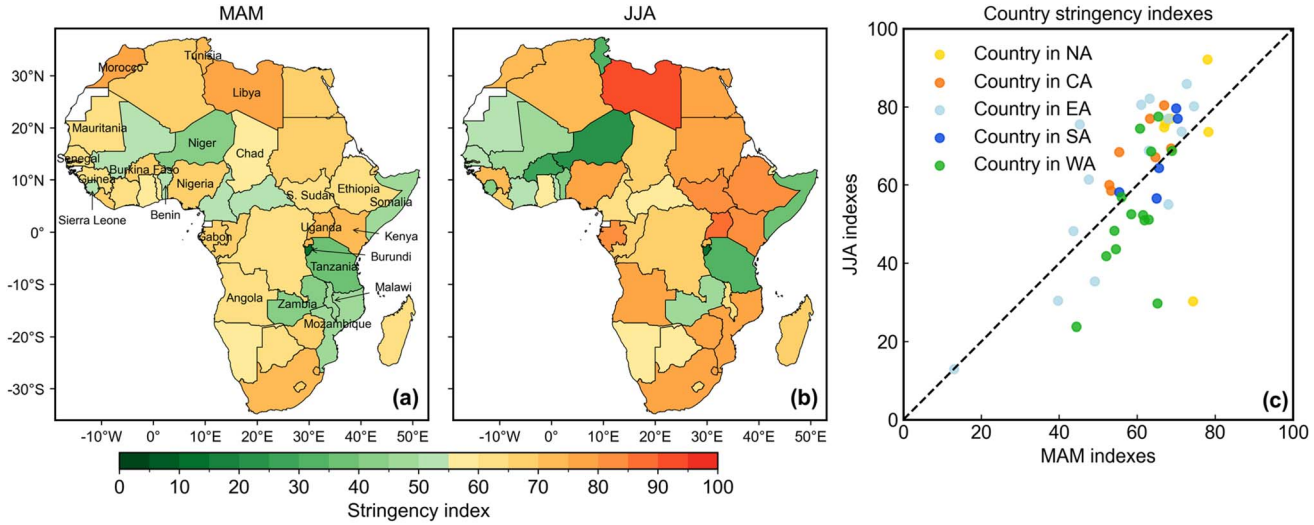

Fig. 1 The stringency index weighted average in major African countries in MAM (a) and JJA (b), and the changes from MAM to JJA (c). Among them, the countries in white (a and b) lack containment information.

responses to the COVID-19 crisis overtime at a daily resolution, including school and workplace closings, public transport closings, international travel restrictions, and so on. Fig. 1 shows that the overall stringency index for the African countries such as Mozambique, Ethiopia, South Sudan, Libya, Malawi, Guinea, Uganda and Nigeria is higher during the JJA season than in MAM, indicating that lockdown measures were generally more stringent in those countries. As shown in Fig. 1c, the stringency indexes of all CA countries have increased in the JJA compared to the MAM, while other regions in Africa have mixed changes. There were 18 countries where the stringency index in the MAM was higher than those in the JJA. These countries include Tunisia, Burkina Faso, Niger, Somalia, Mauritania, Sierra Leone, Senegal and Benin. In MAM, the countries with the highest stringency index include Morocco (78.4), Libya (78.2), Kenya (74.5), Tunisia (74.5), Uganda (72.9), while in JJA, Libya (92.1), Uganda (86.0), South Sudan (82.2), Ethiopia (80.6) and Gabon (80.6) had the highest stringency index (Table S1). It is interesting to notice that countries with lower stringency index which were below 50, such as Burundi, Niger, Tanzania, Zambia, and Somalia (Table S1), had generally released their restriction earlier, which mean that they usually had a higher stringency index in MAM than in JJA (Fig. 1c).

2.3 Surface air quality data

For this study, the long-term chemical reanalysis products constructed by NASA Jet Propulsion Laboratory (https://tes.jpl.nasa.gov/tes/chemical-reanalysis/products/two-hourly, last accessed March 10, 2024) were used. The chemical reanalysis products used a multi-component satellite data assimilation system[36] to assimilate the results of CO, NO_2, SO_2, O_3, and HNO_3 measurements from multiple satellites, including Aura/OMI, Aura/MLS, Aqua/AIRS, Terra/MOPITT, and Suomi NPP/OMPS. Data assimilation uses MICROC-CHASER predictive models to simulate various processes, including transport, emissions, deposition, and chemical reactions such as ozone and aerosol processes. An Integrated Kalman filtering technique was employed to combine prior data (predictions) and observational data for obtaining optimal state estimation.[38] During the optimization of pollutant emission estimates, only total combined emissions were optimized, while proportions of different emission categories from previous emission estimates were applied at each grid point to obtain assimilated posterior anthropogenic emissions.[19] Prior surface NO_x and SO_2 emissions in 2020 were derived from the Hemispheric Transport of Air Pollution version 2.2 at a resolution of 0.1° for the anthropogenic emission (Janssens-Maenhout *et al.*, 2015), Global Fire Assimilation System version 1.2 at a resolution of 0.1° for the fire emissions,[39] and Global Emissions Initiative at a resolution of 0.5° for the soil NO_x emission.[39–41] Lightning NO_x sources in the model were calculated using corresponding parameterizations at each model time step.[42] The emissions in 2020 were constrained by various satellite measurements including NO_2, SO_2, CH_4, CO, and ozone (O_3), with the quality of the reanalysis field evaluated using ozone detection as well as aircraft and satellite observations. Based on TROPOMI NO_2 constraints at a resolution of 0.56°, ground-level NO_x emissions in 2020 have been used to assess global tropospheric ozone response to COVID-19 lockdown measures.[19]

2.4 Tropospheric column data for HCHO and NO_2

To explain the changes in ozone levels in major African countries, high-resolution monthly offline products of HCHO and NO_2 vertical column densities (VCD) for the year 2020 were obtained from the Tropospheric Emission Monitoring Internet Service (TEMIS; https://www.temis.nl/index.php, last accessed March 20, 2024).[43] The TROPOMI Level 3 HCHO and NO_2 data were retrieved using algorithm versions 1.1.2 (HCHO) and 1.2.2 (NO_2), based on the DOAS method with corrections for clouds, aerosols, and surface reflectance to improve accuracy.

Bilinear interpolation was applied to standardize the data resolution to 0.1° × 0.1°. The African border shapefile was then used to extract monthly and quarterly mean concentrations of HCHO and NO_2 across the main continent of Africa. Finally, the HCHO/NO_2 ratios for MAM and JJA in 2020 were calculated.

2.5 Statistical analyses to quantify the air quality changes

For this study, two distinct methods were applied to quantify air quality changes during the lockdown periods. Following previous research (such as Chen *et al.*;[44] Li *et al.*;[45] Ma *et al.*[46] and Zhang *et al.*[47]), the quarterly dual anomalies method, also known as the difference-in-differences method, was first utilized to account for seasonal and long-term variations in air pollution. Specifically, for each country and grid cell in Africa, the air quality changes were calculated during the lockdown period compared with the pre-lockdown period (February) in 2020 and then these changes were compared to those observed during the corresponding periods from reference years (2005–2019). These changes represent the rate of change in pollutant concentrations during the lockdown period compared to pre-lockdown levels. Another method employed is the quarterly anomalies, which was used to calculate seasonal concentration differences between 2020 and the multi-year mean (from 2005 to 2019). The quarterly anomalies were calculated for MAM and JJA separately. Additionally, the rate of change in pollutant concentration for each country was reported, calculated by dividing the quarterly anomalies by the multi-year mean. To further analyze seasonal changes in major air pollutants from 2005 to 2019, the Mann–Kendall trend analysis was performed (Fig. S3). The results indicate that all *P*-values were greater than 0.05 for Africa, suggesting no significant air quality trends attributable to anthropogenic emissions or meteorological conditions during this period. Therefore, it is assumed that the multi-year average from 2005 to 2019 serves as a representative baseline for hypothetical air quality in 2020 had no lockdown measures been implemented, with the calculated quarterly anomalies primarily reflecting emission changes resulting from lockdown measures. To test this hypothesis, air quality changes were also examined by calculating the differences between 2020 values and a five-year average from 2015 to 2019 for both methods. Similar spatial patterns of air quality changes were observed (Fig. S4–S10).

To evaluate the statistical stability of the quarterly dual anomalies and quarterly anomalies methods across countries, we employed a *t*-distribution-based confidence interval estimation.[48] For each country, we first calculated the mean ($\bar{x}$) of the quarterly anomalies, then determined the standard deviation and standard error using the following formulae:

$$s = \sqrt{\frac{1}{n-1}\sum_{i=1}^{n}(x_i - x)^2} \quad (1)$$

$$\mathrm{SE} = \frac{s}{\sqrt{n}} \quad (2)$$

where s is the sample standard deviation (with a degree of freedom of $n - 1$), SE is the Standard Error, x_i stands for a specific value of quarterly dual anomalies or quarterly anomalies, and n is the number of quarterly dual anomalies or quarterly anomalies for the respective country.

Then, the critical value of the confidence interval is further calculated: with a confidence level of 95%, the critical value t^* is determined as follows:

$$t^* = t_{0.975}\ (\mathrm{df} = n - 1) \quad (3)$$

where $t_{0.0975}$ is the critical value of the two-tailed *t*-distribution with $n - 1$ degrees of freedom. We then calculate the upper and lower bounds of the confidence interval ($\mathrm{CI_{lower}}$, $\mathrm{CI_{upper}}$) as well as its half-width ($\mathrm{CI_{half}}$):

$$\mathrm{CI_{lower}} = \bar{x} - t^{*}\cdot \mathrm{SE} \quad (4)$$

$$\mathrm{CI_{upper}} = \bar{x} + t^{*}\cdot \mathrm{SE} \quad (5)$$

$$\mathrm{CI_{half}} = t^{*}\cdot \mathrm{SE} \quad (6)$$

Statistical stability is determined using a dynamic threshold. Let the set of confidence interval half-widths for all countries be denoted as $\mathrm{CI_{half}}^{(1)}$, $\mathrm{CI_{half}}^{(2)}$,.... By calculating the median (M) and interquartile range (IQR) of this set, the stability threshold is defined as:

$$\mathrm{Threshold} = M + 1.5\cdot \mathrm{IQR} \quad (7)$$

If the confidence interval half-width ($\mathrm{CI_{half}}$) of a country is less than or equal to the threshold, the average value of that country is considered representative of the variation level across the entire country.

2.6 Random forest model prediction of pollutants

To isolate the influence of local meteorological changes, a random forest (RF) model was applied to predict pollutant concentrations in specific regions of Africa, with a focus on Central African countries that have experienced a significant decrease in CO levels. Random Forest is an ensemble learning method that combines multiple decision trees to improve prediction accuracy and robustness. It uses two types of randomness: bootstrap sampling to create different training sets for each tree, and random feature selection for each split. This reduces overfitting and increases model diversity. The final prediction is made by voting (for classification) or averaging (for regression). Random Forest is effective at handling large datasets, high-dimensional data, noise, and missing values, offering strong accuracy and stability.[49] The average daily values of each feature from February to August 2015–2019 were utilized as the training set for this analysis. The features included time (the day of the year), latitude and longitude, as well as meteorological variables such as temperature (T_2), humidity, v wind and u wind. The target variable was the CO concentration. All of the data are from the chemical reanalysis products constructed by NASA Jet Propulsion Laboratory (https://tes.jpl.nasa.gov/tes/chemical-reanalysis/products/two-hourly, last accessed March

10, 2024) and the resolution was uniformly adjusted to 0.5° × 0.5° using bilinear interpolation. These predictions are based on historical levels of CO, which include information on past anthropogenic emissions. Therefore the predicted CO concentrations still retain the influence of emissions from previous years. To improve accuracy, simulations were conducted for February, MAM, and JJA separately. For model validation, a time series split rolling cross-verification was employed based on five splits according to Shen *et al.*[50] The performance of the model was measured using the Pearson correlation coefficient (PCC) and low root mean square error (RMSE), as shown in Fig. S14. After cross-validation (Fig. S18), the optimal model was selected to predict the CO concentrations in 2020 under the previous emission scenario. The "n_estimators" of the model was 108 and "max_depth" was 21. Then, by subtracting the actual CO concentrations in 2020 from the predicted values, we can isolate the air quality changes from the meteorological conditions. Finally, we calculated the average concentrations of CO for February, MAM, and JJA respectively.

2.7 Pearson correlation analyses

Pearson correlation analysis was conducted to examine the relationships between pollutants and the stringency index or meteorological variables.[51] Average daily concentration anomalies for SO_2, CO, NO_2, temperature, and absolute humidity were calculated for the period from March 1 to August 31, 2020. The calculations of the average daily concentration anomalies were similar to the quarterly anomalies we described above. Then, the Pearson correlation coefficients of pollutant daily anomaly with temperature daily anomaly, absolute humidity daily anomaly and the stringency index were calculated from

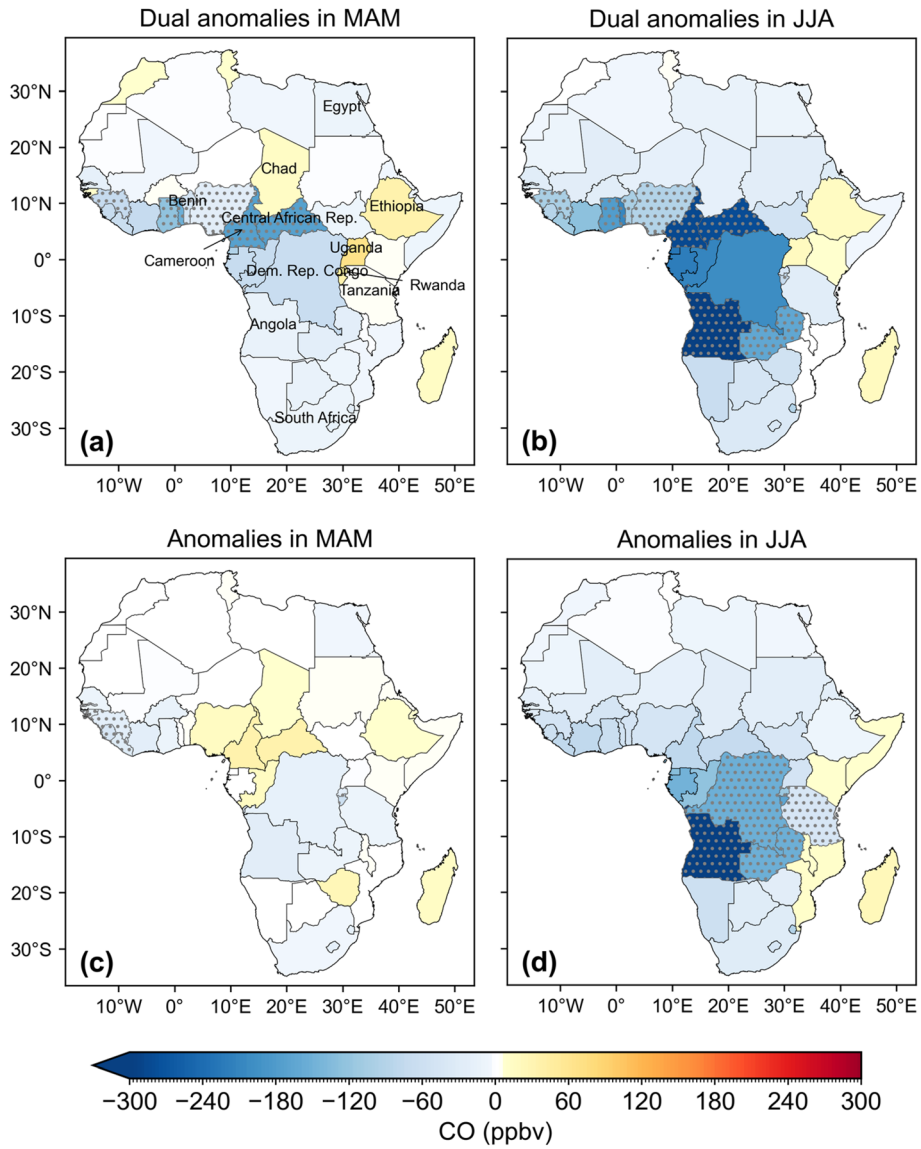

Fig. 2 Spatial distribution of CO changes from the two methods: quarterly dual anomalies (a and b), and quarterly anomalies (c and d) for MAM (a and c), JJA (b and d) in African countries. The units are ppbv. For countries marked with gray dots, their national average values cannot represent the situation of the entire country. White denotes countries where the change falls below 2% of the minimum value observed.

March 1 to May 31 and from June 1 to August 31, respectively. The results are shown in Fig. 3 and S19–S21.

3 Results

3.1 Gas pollutant change for CO, SO_2, and NO_2

3.1.1 CO changes. Fig. 2 shows the spatial distribution of CO changes in MAM and JJA in African countries estimated from the two methods. In general, we found consistent temporal–spatial CO changes from the two methods, with larger CO decreases observed in JJA than those in MAM, sharing the similar spatial patterns with the country stringency index (Fig. 1). The average CO changes in Africa were −54.92 ppbv (−469.60 to 22.46 ppbv depending on the country) in Africa during the JJA and −0.10 ppbv (−61.51 to 33.85 ppbv) in MAM (Fig. 2c and d). Meanwhile, the two methods are consistent in showing that the countries with the largest CO decline are mainly located in CA, such as Angola (Fig. 2b and d). Previous studies have shown that 90% of fires that occurred in sub-Saharan regions were caused by human activities,[52,53] especially in JJA, which is the fire season in the southern hemisphere (Fig. S22). Analysis of fire radiative power (FRP) data (Fig. S23) shows that FRP in 2020 was lower than in previous years across Central African countries (*e.g.*, Angola, the Central African Republic, and the Democratic Republic of the Congo). Specifically, the Central African Republic recorded an MAM FRP decline outside natural variability compared to the 2015–2019 annual average, with falling approximately 2.8 standard deviations below the 2015 to 2019 average FRP. Changes in FRP in other countries, such as Cameroon, were also consistent with variations in CO concentrations. Thus, it can be concluded that the constrained human activities during the strict lockdown periods in JJA (Fig. 1) reduced the occurrence of wildfires[54] and led to a more significant CO decline. Zhang and Zhang (2025)[55] also identified wildfires and climate change as key drivers of forest carbon flux variations in Africa over the past two decades, noting that compared to wildfires, the impacts of these climate drivers are slower and more spatially variable. Furthermore, light-duty vehicles were another major source of CO especially in the Sahara regions such as Egypt in NA,[33] indicating that the stricter lockdown measures which restrained the vehicle's activities contributed to reducing the CO concentration.[56] Besides the similar results we drew from the two methods, there are slight variations, with the quarterly dual anomalies method (Fig. 2a and b) usually showing larger CO decreases in both seasons. Also, the significant CO decreases in Cameroon and Central African Republic were observed in both seasons using the quarterly dual anomalies (Fig. 2a and b). In contrast, reductions were not detected by the quarterly anomalies method (Fig. 2c and d). We also found obvious CO increases in MAM especially in NA regions as estimated from the quarterly anomalies method (Fig. 2c). This could be caused by the high natural biomass burning activity in the Northern hemisphere of Africa[57] and the low population (Fig. S24). To further investigate the contribution of emission changes to the concentration anomalies in 2020, we compared the CO concentration differences in MAM and JJA of 2020 between those estimated in the chemical reanalysis data with the RF-predicted CO concentration which isolated the influence of meteorological changes, and a similar magnitude change between these two was found, confirming the conclusions above (Fig. S25).

By calculating the Pearson correlation coefficient between CO anomalies and stringency index (Fig. 3), it was found that during the MAM, many countries exhibited a significant negative correlation between these two variables. This negative correlation was mainly concentrated in CA, WA and NA, such as

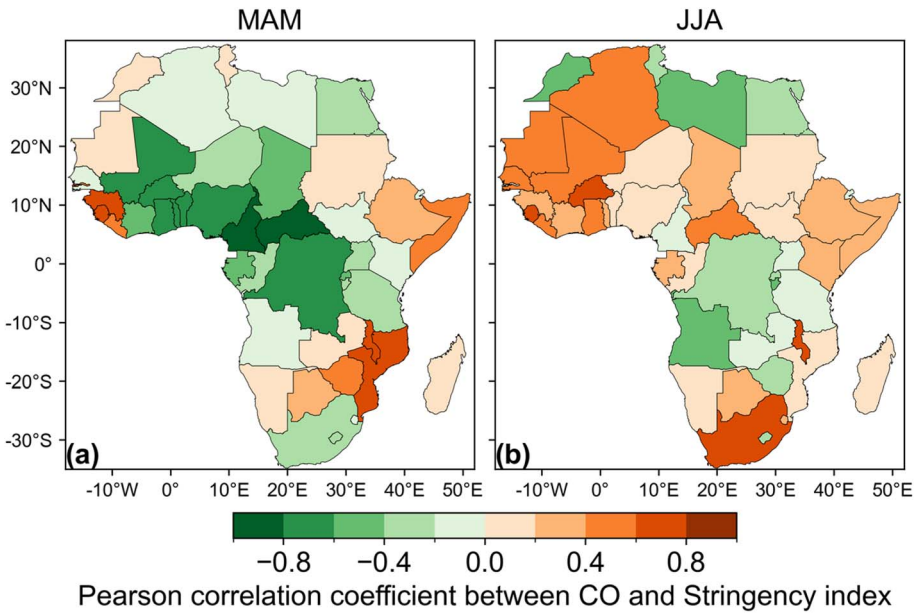

Fig. 3 Spatial distribution of Pearson correlation coefficients from March 1st to May 31st (a), and June 1st to August 31st (b) in African countries. Positive values denote positive correlations and negative values denote negative correlations between daily CO anomalies and the stringency index.

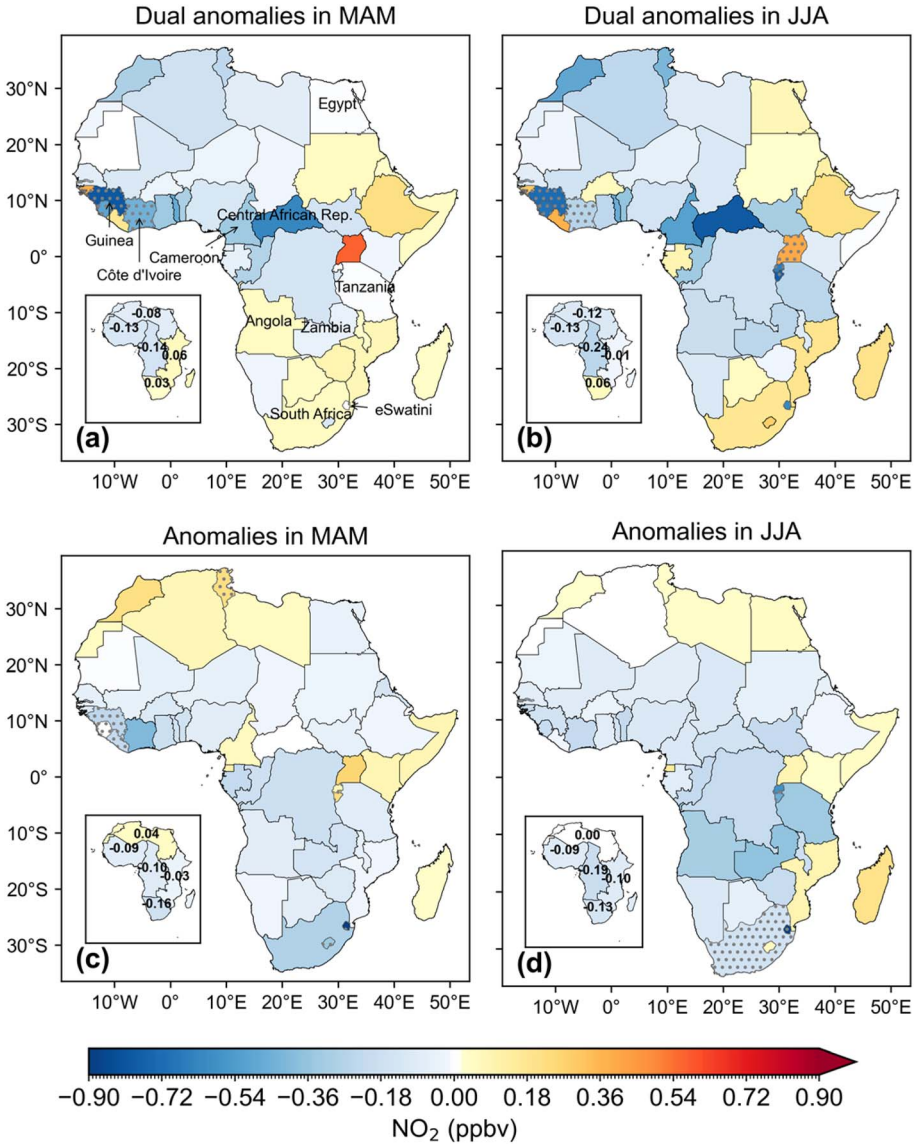

Fig. 4 The same as Fig. 2, but for NO_2. The inserted plot displays the average values across five African regions. Quarterly dual anomalies (a and b), and quarterly anomalies (c and d) during MAM (a and c) and JJA (b and d) in African countries. The units are ppbv.

the Central African Republic, Cameroon, Nigeria, Egypt and South Africa. Although the Central African Republic had moderate lockdown stringency indexes and population levels, its CO concentration still significantly decreased due to its originally higher CO concentration, leading to more noticeable emission reductions. In contrast, despite lower original CO concentrations in Egypt and South Africa, their higher stringency indexes resulted in a decrease in CO concentrations. However, countries like Chad, Uganda, and Ethiopia still had positive dual anomalies, which may be related to lower stringency indexes in these countries or their neighbours, as well as meteorology. During the JJA, the decrease in CO concentrations was negatively correlated with stringency indexes in some countries only, particularly in CA and NA. Because some countries have a lower level of stringency index during the JJA, the Pearson correlation analysis may be affected by unusual occasional changes in pollutants. In conclusion, changes in CO concentration are co-controlled by each country's individual CO emission levels, the lockdown stringency indexes and even population conditions.

3.1.2 NO_2 change. As shown in Fig. 4, the spatial NO_2 anomalies in MAM and JJA estimated from the two methods agree well with each other, similar to what was observed for CO. The reduction in NO_2 concentration in CA and WA regions is attributed to reduced biomass burning and industrial emissions due to strict lockdown measures as also discussed in previous studies.[58,59] In some countries such as Central African Republic and Cameroon, the decreases in NO_2 during JJA were slightly larger than those during MAM. This aligns with the overall trends in the stringency index between the two seasons. In general, the average change in NO_2 across Africa during JJA is −0.09 ppbv (−1.8 to 0.2 ppbv, corresponding to a change rate of −29.9% to 30.1% depending on the country; see Fig. S27b), whereas during MAM, the average change is −0.05 ppbv (−1.2

to 0.3 ppbv, change rate between −38.8% and 23.4%). Some countries, such as Egypt, Chad, and Tanzania, showed similar changes from both methods. In SA, the quarterly anomalies method showed an obvious decrease in NO_2 which was not captured by the quarterly dual anomalies method.

However, for parts of NA and SA, the NO_2 trends derived from the two methods differ (and even contradict with each other). For example, the quarterly dual anomalies showed NO_2 decreases in NA countries, such as Tunisia, Morocco, Algeria, and Libya, whereas the quarterly anomalies method showed an increase. This shows that while NO_2 levels in some countries of NA have increased compared with previous years, the magnitude of the increase is smaller than that observed before the lockdowns. In contrast, for SA countries (such as South Africa and Botswana), the quarterly dual anomalies showed an increase in NO_2, whereas the quarterly anomalies method indicated a decrease. This implies that even though NO_2 concentrations have increased relative to the pre-lockdown period, the magnitude of the increase is lower than that in normal years. After the lockdown, some countries may have retained certain environmental control measures (*e.g.*, traffic restrictions, promotion of clean energy). These measures have curbed the rebound rate of NO_2 concentrations, resulting in a weaker recovery trend than in previous years. However, during the lockdown period, due to demands such as heating and capacity adjustments in some high-emission industries in these southern countries, particularly during JJA, the emission intensity after resumption of work and production may have been inherently lower than that before the lockdown, which in turn is reflected as an insufficient rebound in concentration. In addition, the countries showing the greatest declines differ between the two methods. The quarterly dual anomalies method shows the largest NO_2 decreases that occurred in WA and the northern parts of CA during MAM and JJA, such as in

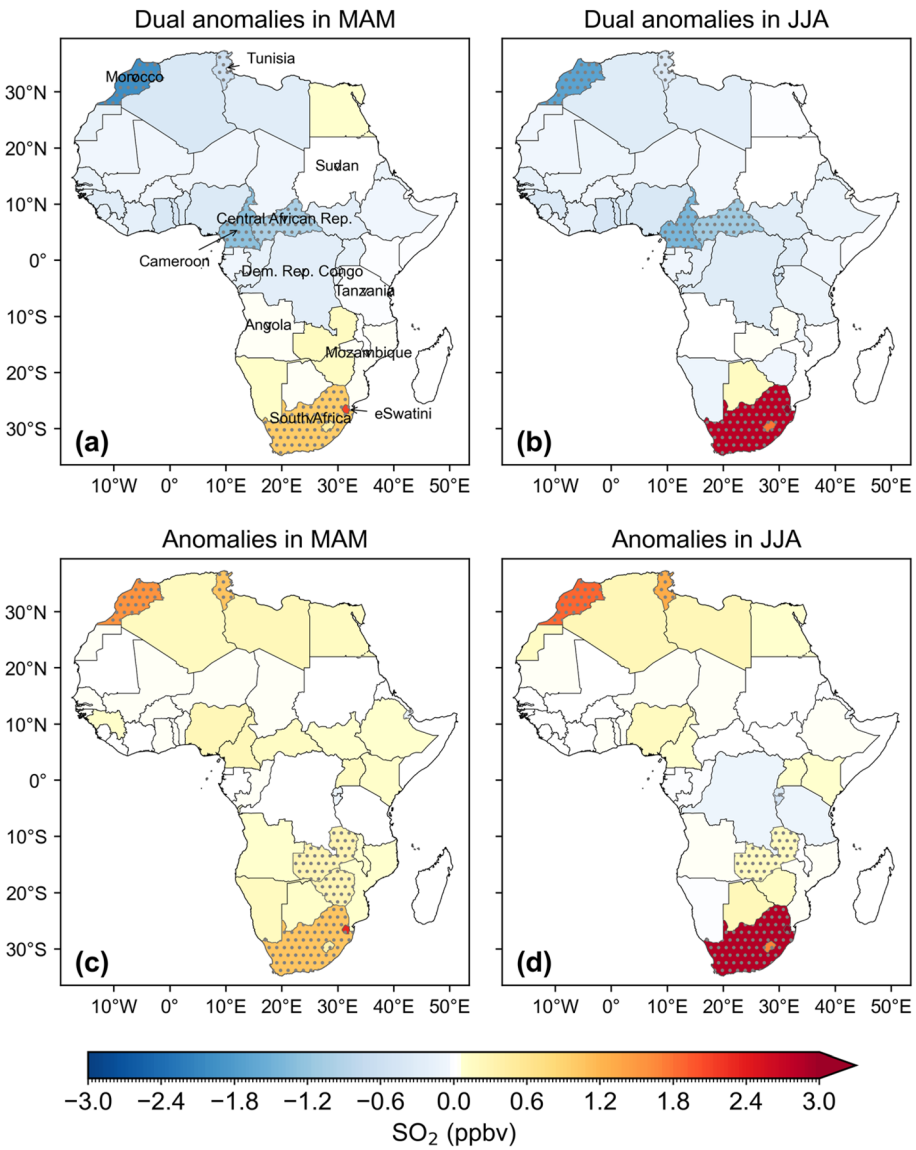

Fig. 5 The same as Fig. 2, but for SO_2. Quarterly dual anomalies (a and b), and quarterly anomalies (c and d) during MAM (a and c) and JJA (b and d) in African countries.

the Central African Republic (−0.6 and −0.8 ppbv), Cameroon (−0.3 and −0.5 ppbv), and Guinea (−0.8 and −0.7 ppbv). Conversely, the quarterly anomalies method shows the greatest declines in NO_2 concentration in southern parts of CA and SA, such as Eswatini (−1.2 ppbv), South Africa (−0.3 ppbv), and Côte d'Ivoire (−0.4 ppbv) in MAM, and Eswatini (−1.8 ppbv) and Angola (−0.3 ppbv) in JJA. This indicates that while NO_2 concentrations have decreased in these countries, the rate of decline is relatively slow, and heating during the cold season has mitigated this downward trend.

3.1.3 SO_2 change. Fig. 5 illustrates the spatial distribution of SO_2 changes in MAM and JJA as estimated by two methods in African countries. Surprisingly, there is substantial and even contradictory variation in SO_2 concentration changes between the two methods. The dual quarterly anomalies methods showed a general decrease in SO_2 (Fig. 5a and b), led by Morocco (−1.62 ppbv), Cameroon (−1.45 ppbv), and the Central African Republic (−1.21 ppbv). However, the quarterly anomalies indicate widespread increases in SO_2 concentration in both seasons (Fig. 5c and d), with slightly noticeable decreases in countries like the Democratic Republic of Congo and Tanzania during JJA. This difference is attributed to the quarterly anomalies method indicating the rate changes at which the concentration of pollutants decreases or rises during the lockdown period compared with those during pre-lockdown. We found higher SO_2 concentration in the WA and NA in Feb 2020, which makes the relative comparisons with MAM and JJA in 2020 much lower. However, the anomalies method only considered the changes between 2020 and previous years. When the two methods are considered in combination, the results indicate that although SO_2 concentrations in most African countries increased in 2020 compared with previous years, the growth rate was slower than that observed before the lockdown measures were

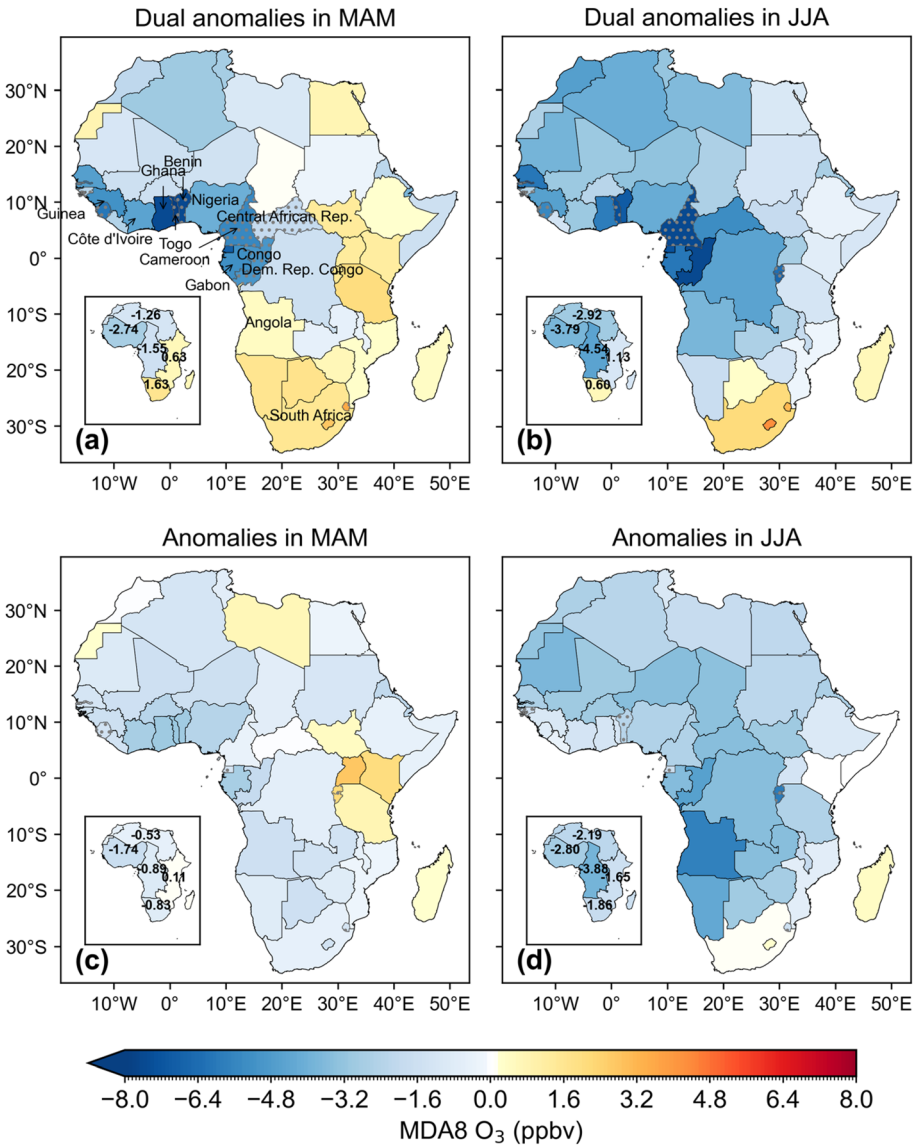

Fig. 6 The same as Fig. 2, but for MDA8 O_3. The inserted plot displays the average values across five African regions. Quarterly dual anomalies (a and b), and quarterly anomalies (c and d) during MAM (a and c) and JJA (b and d) in African countries.

implemented. This indirectly demonstrates the effectiveness of the lockdown policies.

In addition, both methods indicated that in SA countries such as South Africa and Mozambique, the concentration of SO_2 continued to increase, which contradicts the stringency index change. This increase is attributed to the possible expansion of coal-fired power plants in these countries.[60,61] On April 1st, 2020, this region doubled the emission limit for SO_2 from coal-fired power plants and allowed many factories to reopen after July 1st.[37,60] Besides, stay-at-home policies may lead to an increase in residential electricity demand and the use of fuels for activities such as cooking and heating,[62–64] thereby increasing the operating load of power plants[65] and then SO_2 concentrations. Meanwhile, the dry, cold conditions in the Southern Hemisphere make it harder for SO_2 to disperse. Previous studies have observed that, apart from Africa, in some countries with high SO_2 emissions such as Turkey[66] and India,[13] certain cities also experienced an increase in SO_2 concentrations during lockdown periods.[13,67,68] This highlights the need for stricter coal restriction policies or promotes the use of clean energy to reduce environmental pollution in these regions. Therefore, containment policies implemented in winter may have a limited effect on SO_2 reduction in regions with heavy coal-burning industries and residential burning. Additionally, during the MAM, over half of the countries also exhibited negative correlations between NO_2, SO_2, and the stringency index (Fig. S19 and S20). Specifically, in Chad (−0.84) and the Central African Republic (−0.83), the correlation coefficients between NO_2 variations and the stringency index fell below −0.8. For SO_2, Cameroon recorded a correlation coefficient of −0.90. By the JJA season, the correlation coefficients weakened (became less negative) for most countries. This indicates that strict lockdown measures effectively mitigated the increase in NO_2 and SO_2 emissions in most regions. Although lockdown measures were relaxed during the JJA season, the combined influence of various conditional factors still contributed to the declining trend of NO_2 and SO_2 concentrations in the majority of countries.

3.2 Ozone change

As shown in Fig. 6, both methods indicated a larger decline for the maximum daily 8 hour average (MDA8 O_3) in Africa during JJA than those during MAM. The JJA anomaly is −2.48 ppbv (−5.98 to 0.35 ppbv), ranging from −11.67% to 1.08%, compared with a −0.74 ppbv (−3.12 to 2.74 ppbv, ranging from −10.99% to 7.54%) decrease in MAM (Fig. S29). Both methods agree with each other on the regions with the greatest declines. During MAM, the largest declines occurred in the WA region, such as Togo (−9.37 from the dual anomaly method and −3.12 ppbv for the anomaly method), Benin (−7.66 and −2.92 ppbv), and Ghana (−7.56 and −2.96 ppbv). In JJA (Fig. 6b and d), countries in CA such as Congo (−7.64 and −4.57 ppbv for the dual anomaly and anomaly method respectively), Gabon (−6.03/−3.59 ppbv), and Central African Republic (−5.40/−3.47 ppbv) exhibited the most significant decreases, which had hot spots (Fig. S28). In regions with frequent biomass burning such as WA and CA, the decline in O_3 concentrations may be more closely related to reduced biomass burning emissions due to lockdown measures. We employed the ratio of satellite-derived HCHO (representing VOCs) to NO_2 as an indicator to assess O_3 sensitivity to precursors in Africa.[69–71] We found that in many countries across WA (such as Togo, Ghana, and Benin), Central, and EA, anomalies in O_3 concentrations corresponded well with changes in NO_2 (Fig. 7). This alignment is attributed to higher levels of VOC/NO_x ratios in regions with abundant tropical vegetation, where O_3 tends to correlate positively with NO_x.

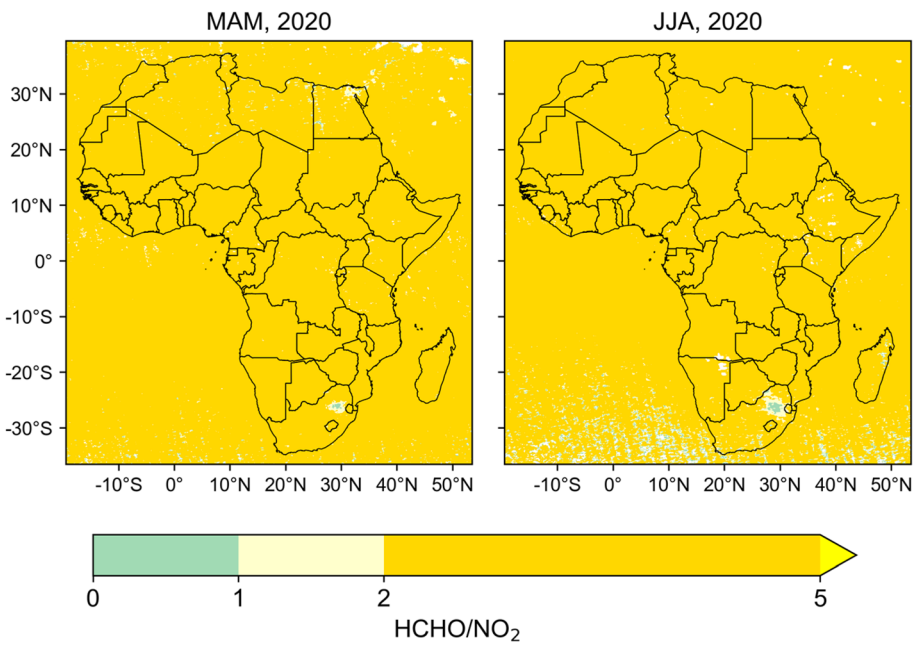

Fig. 7 Spatial distribution of averaged HCHO/NO_2 ratios during MAM and JJA, 2020.

In South Africa, both methods showed a greater increase in O_3 concentrations during the JJA compared to MAM (Fig. 6), which may be associated with a decline in NO_2 concentrations. According to Fig. 7, during the JJA, industrial areas of South Africa exhibited broader ranges of lower HCHO/NO_2 ratio, indicating a negative correlation between O_3 and NO_x.[72] Significant reductions in NO_x levels favor O_3 formation.[73] Additionally, strong correlations between O_3 and CO in South Africa have been reported,[74] and Vakkari *et al.*[75] documented rapid O_3 formation in plumes from grassland fires in South Africa, highlighting the substantial influence of biomass burning emissions on O_3 generation in SA. The O_3 increases during the lockdown were also seen in some regions of other countries, such as Shanghai,[7] North China[76] and Milan in Italy.[77]

In both methods, a widespread decrease in surface O_3 across NA was observed, possibly influenced by ozone precursors and meteorological conditions, particularly temperature.[78] Compared with previous years, temperatures in the Sahara have notably decreased, particularly during JJA, with coastal regions experiencing a decline of 4 °C (Fig. S31c). Lower temperatures might reduce the photolysis rate of ozone molecules, further stabilizing the atmosphere and making it less likely for O_3 to disperse, thereby leading to decreased surface O_3 concentrations.

3.3 Aerosol particles

The inorganic aerosol concentration changes, including sulfate, nitrate and ammonium aerosols, often exhibit nonlinear relationships due to their formation through both primary emissions and secondary reactions of gaseous precursors in the atmosphere.[79,80] Etchie *et al.*[81] found that meteorological conditions rather than lockdowns resulted in marginal reductions in aerosol levels in Nigeria. Similar observations of no

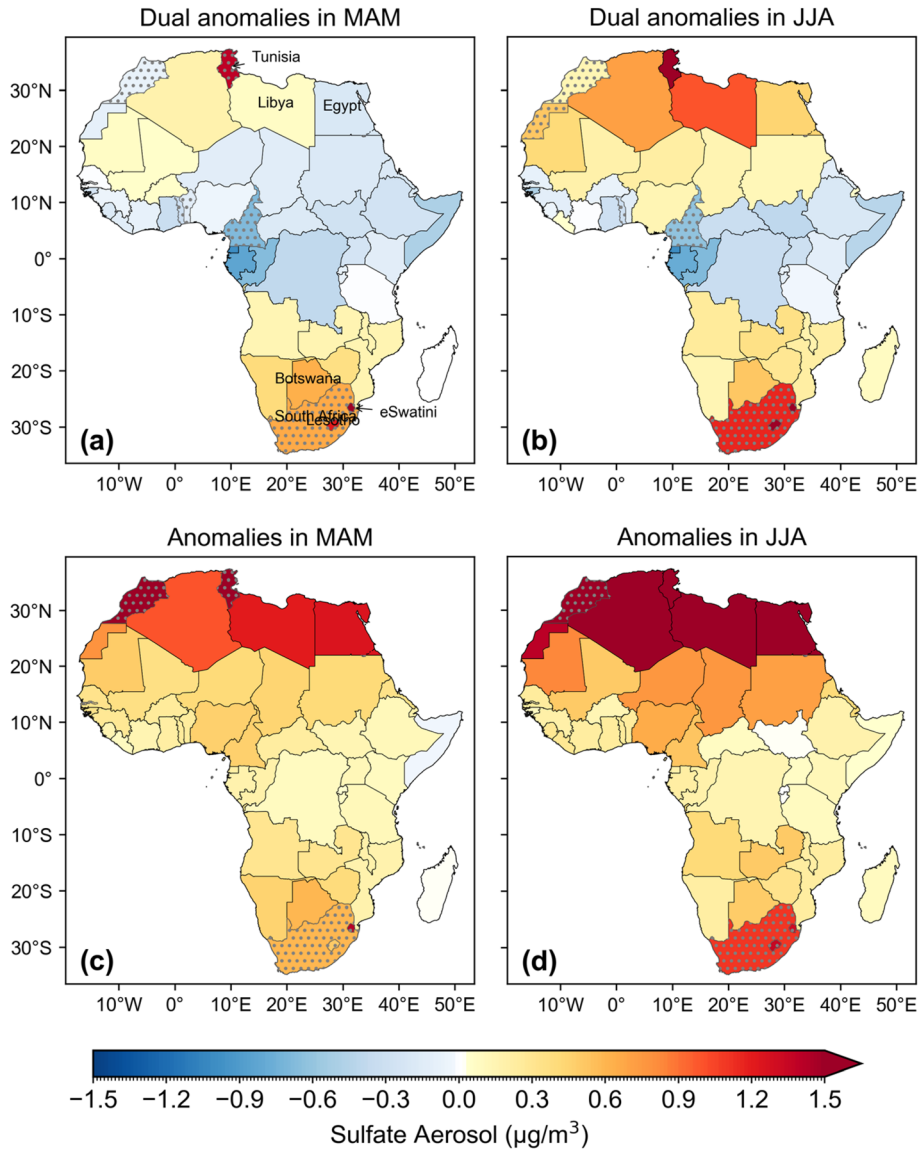

Fig. 8 The same as Fig. 2, but for sulfate aerosol. Quarterly dual anomalies (a and b), and quarterly anomalies (c and d) during MAM (a and c) and JJA (b and d) in African countries.

significant reductions in atmospheric particulate matter due to lockdown measures have also been reported in China, the United States, Spain and India.[16,82–85]

Unlike other pollutants, both methods showed a greater increase for sulfate aerosols in JJA compared to MAM across Africa overall, especially in NA and SA (Fig. 8). The average sulfate aerosol particles in Africa were estimated to be 0.49 μg m^{-3} and 0.72 μg m^{-3} for MAM and JJA respectively from the quarterly anomaly method. NA, located in the Sahara Desert, is the world's largest dust source.[86] The increase in sulfate aerosol concentration was primarily influenced by Saharan dust storms in June 2020. Burgess and Oyola-Merced[87] have shown that the concentration of sulfate aerosols in the atmosphere over Africa significantly increases during Saharan dust storms. Furthermore, the decrease in temperature and humidity during the JJA in NA regions compared to previous years also favours the accumulation and transport of aerosols,[88,89] thereby increasing aerosol particle concentrations. In SA, the significant increase in sulfate, particularly in South Africa, may be linked to increased coal combustion activities during lockdown periods. However, the two methods showed distinct results for sulfate aerosol changes in WA, CA and EA regions, observed for the gaseous SO_2 (Fig. 5). The quarterly dual anomaly displayed an overall decrease in concentrations in these regions (Fig. 8a and b), whereas the quarterly anomaly shows a slight increase (Fig. 8c and d). This is linked to the elevated February concentrations of sulfate aerosols near the equator compared to previous years (Fig. S12d). The comprehensive analysis of both methods suggests that despite a relative increase in sulfate aerosol concentrations compared to previous years (Fig. S14a and d), reduced fires due to pandemic lockdowns or meteorological conditions can mitigate the upward trend in sulfate concentrations. Similar to sulfate aerosol, we observed an increase in ammonium aerosol in both MAM and JJA in most

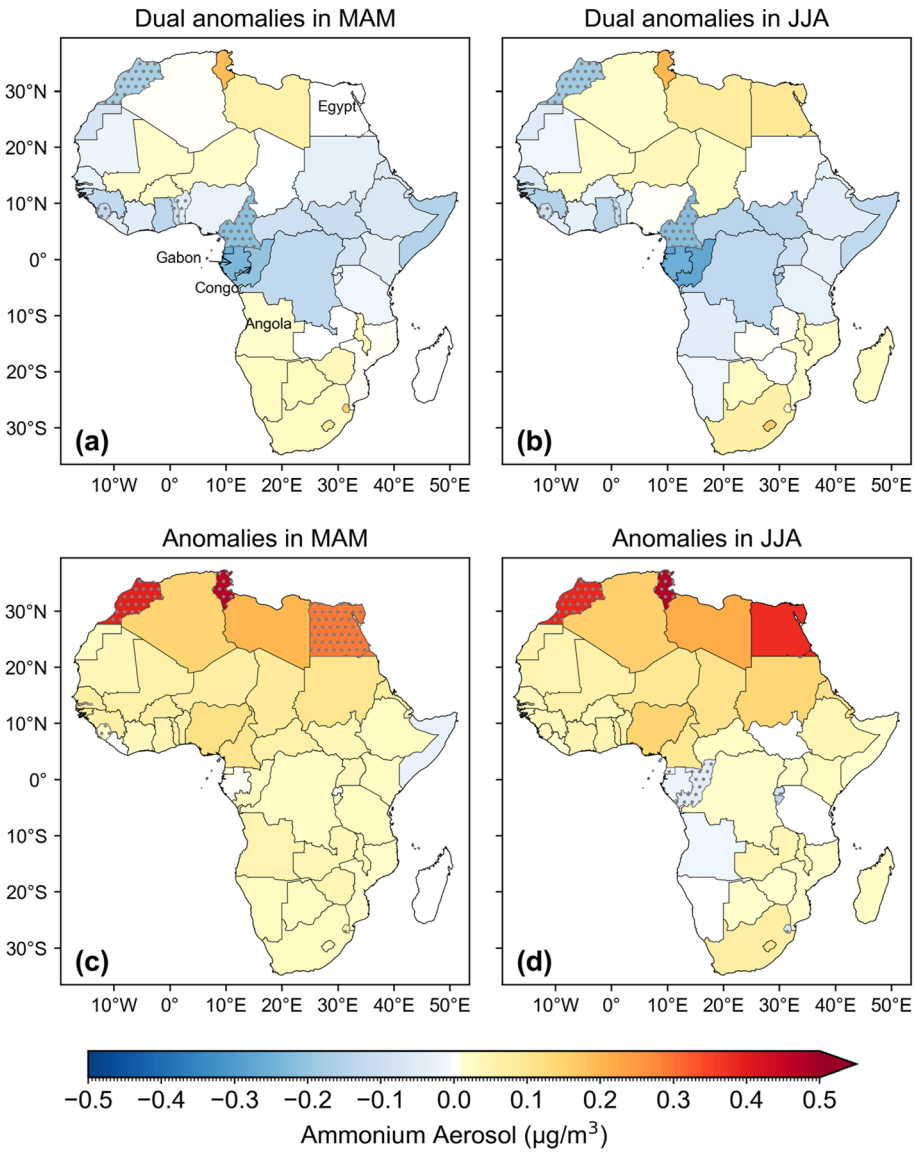

Fig. 9 The same as Fig. 2, but for ammonium aerosol. Quarterly dual anomalies (a and b), and quarterly anomalies (c and d) during MAM (a and c) and JJA (b and d) in African countries.

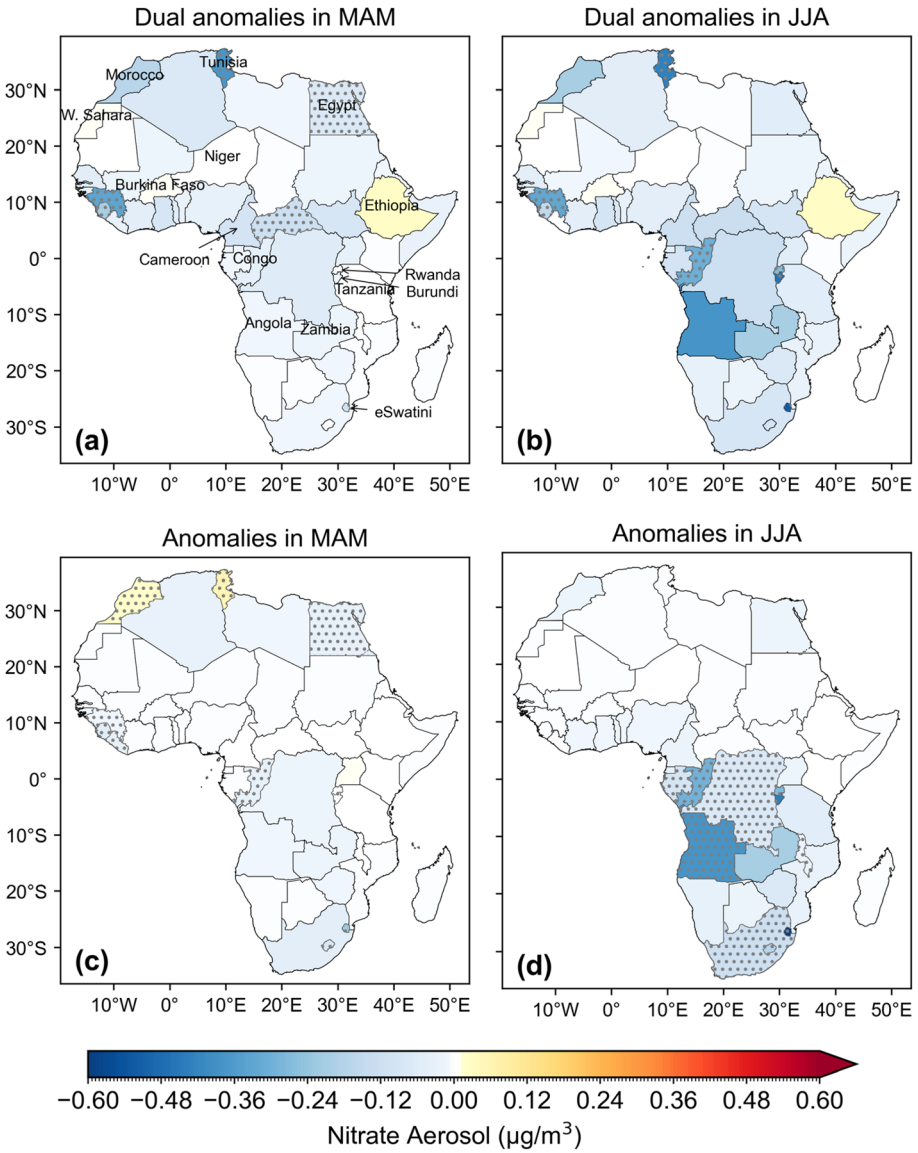

Fig. 10 The same as Fig. 2, but for nitrate aerosol. Quarterly dual anomalies (a and b), and quarterly anomalies (c and d) during MAM (a and c) and JJA (b and d) in African countries.

countries (Fig. 9), especially in the NA and SA regions. This led us to conclude that ammonium existed mostly in the form of ammonium sulfate,[90,91] and was therefore influenced by biomass burning and soil emissions (*e.g.*, animal manure, fertilizers).[13,92]

As shown in Fig. 10, unlike sulfate and ammonium aerosols, the nitrate aerosol showed consistent decreases from the two methods in major African countries. For instance, using the quarterly anomalies method, the average MAM anomaly in Africa is −0.01 μg m^{-3}, ranging from −0.23 to 0.06 μg m^{-3} (−89.45% to 114.27%, Fig. S31), while the JJA anomaly is −0.04 μg m^{-3}, ranging from −0.64 to 0.004 μg m^{-3} (−74.50% to 47.22%). Both methods showed a greater decrease in JJA compared to MAM across Africa, particularly in countries such as Angola, Zambia and Eswatini. Relative to other aerosol particles, nitrate aerosol particles primarily depend on emissions of nitrogen oxides from human activities in the atmosphere, such as traffic, industrial activities, and construction.[61] Therefore, during the pandemic, restricted traffic measures from lockdown led to more pronounced reductions in nitrogen dioxide levels, thereby affecting nitrate aerosol production. In regions with higher nitrate, such as Egypt, Tunisia, and Angola (Fig. S15), the magnitude of concentration decrease was also greater, consistent with previous findings.[33] We observed that in some countries with lower stringency index of lockdown measures (such as below 60), such as Niger, Burkina Faso and Ethiopia, pollutant concentrations decreased slowly or even increased. This suggests that in Africa, the wide-ranging decrease in nitrate aerosol concentrations due to lockdown measures may not have been uniformly observed. While NO_2 rebounded due to the recovery of local anthropogenic activities in parts of SA (dual anomalies) and NA (anomalies), the abundant alkaline mineral aerosols introduced by the enhanced dust storms preferentially reacted with oxidized SO_2

to form sulfate. This process likely involved the reactive substrates necessary for NO_2 conversion to nitrate.[93,94] Consequently, coupled with the subsequent sedimentation of dust, the concentration of nitrate exhibited a downward trend.

4 Summary and conclusions

This study analyzed the impact of lockdown policies on the changes in gaseous pollutants in African countries, focusing on CO, NO_2, SO_2, O_3 and aerosol particles. We applied two distinct methods, quarterly dual anomalies and quarterly anomalies to calculate the concentration changes in March to May (MAM) and June to August (JJA) in 2020. The quarterly dual anomalies calculated the air quality changes during the lockdown period compared with the pre-lockdown period (February) and then compared these changes to corresponding periods from reference years (2005–2019). The quarterly anomalies calculated the seasonal concentration differences between 2020 and the multi-year mean (2005–2019) for MAM and JJA individually.

1. Both methods revealed a decrease in CO concentrations in most African countries, with greater reductions observed during JJA compared to MAM. This is attributed to the emission reductions from biomass burning (sub-Saharan) and the transport emissions (Saharan) which were both caused by the restricted human activities during the lockdown.[33,57] The random forest model further corroborated the significant role of anthropogenic emission changes in the observed reduction of CO concentrations in CA.

2. Both methods observed a decrease in NO_2 concentrations across most African countries, with a slightly larger reduction in JJA compared to MAM, demonstrating the effectiveness of restrictions on traffic, biomass burning, and industrial activity. However, discrepancies were observed in the NA region, where the quarterly dual anomalies method indicated a decline in NO_2, while the quarterly anomalies method showed an increase. This suggests that while NO_2 levels were generally higher in February 2020 compared to previous years, containment measures, especially traffic restrictions,[33] mitigated the rate of increase.

3. Unexpectedly, both methods observed an increase in SO_2 in South Africa, especially during JJA. This increase may be linked to relaxed emission limits for factory pollutants and heightened coal-fired power plant usage during home isolation in winter.[37,60] For most other countries, the quarterly dual anomalies method revealed a general decline in SO_2, whereas the quarterly anomalies indicated an increase. This shows that despite an overall increase in SO_2 levels in 2020, containment measures may have slowed the rate of increase.

4. Regarding MDA8 O_3, both methods indicated a general decline in concentrations in most countries, especially in WA and CA regions, with greater reductions observed during JJA. This decline is likely related to reduced emissions from biomass combustion as a result of lockdown measures. However, in South Africa, a more significant increase in O_3 during JJA was noted, potentially due to decreased NO_2 concentrations and lower tropospheric HCHO/NO_2 ratios.

5. Both methods revealed an increase in sulfate and ammonium aerosols in the NA and SA regions, with a larger increase during JJA. In the NA region, this increase is likely associated with an extreme dust event in June 2020, while in the SA region, it corresponds to increased coal burning.[95] Nitrate aerosols consistently decreased across both quarters, reflecting the overall reduction in NO_2 emissions due to containment measures.

In conclusion, the air quality changes during lockdown in Africa may be interweaving with both natural and anthropogenic influences. Judging the similarities and disagreements between the two methods applied in this study, we highlight the necessity to include more surface observations for African countries, as well as stricter emission standards for coal-fired plants and promote clean energy infrastructure. However, due to the scarcity of surface *in situ* observation sites across the African continent, the quantitative interpolation of SNA changes over this region is subject to considerable uncertainties and requires further validation. Nevertheless, to the best of our knowledge, this study represents the first comprehensive attempt to interpolate inorganic aerosol changes over Africa during the COVID-19 period by combining state-of-the-art chemical transport modeling and satellite-based observations.

Author contributions

Zizhen Han: methodology, formal analysis, investigation, software, validation, visualization, data curation, writing – original draft. Yuqiang Zhang: conceptualization, methodology, funding acquisition, validation, writing – review & editing. Zhou Liu: resources, software. Kexin Zhang: resources. Stanley Numbonui Tasheh: writing – review & editing. Narcisse Tchinda Tsona: writing – review & editing. Zhuyi Wang: resources. Bin Luo: software. Likun Xue: writing – review & editing. Xinfeng Wang: writing – review & editing.

Conflicts of interest

The authors declare that they have no known competing financial interests or personal relationships that could have appeared to influence the work reported in this paper.

Data availability

All the data required to assess the conclusions in the paper are present within the paper and/or supplementary information (SI). Supplementary information: a map of the African study region, the trends and seasonal anomaly values of atmospheric pollutants over Africa from 2005 to 2019, partial correlation analysis results between primary pollutants and meteorological conditions, fire radiative power data from 2015 to 2020, and validation results of the machine learning model, among others. See DOI: https://doi.org/10.1039/d5ea00111k.

Code availability: the software code could be made available upon request by contacting the corresponding author.

Acknowledgements

We acknowledge the use of data products from the TROPESS Project (TRopospheric Ozone and its Precursors from Earth System Sounding) which is a NASA-funded activity under the NASA Earth Science Mission Directorate (SMD) program called Ozone Trends Science (OTS).

References

1 E. Pepe, P. Bajardi, L. Gauvin, F. Privitera, B. Lake, C. Cattuto and M. Tizzoni, COVID-19 outbreak response, a dataset to assess mobility changes in Italy following national lockdown, *Sci. Data*, 2020, **7**, 230.

2 C. Navinya, G. Patidar and H. C. Phuleria, Examining Effects of the COVID-19 National Lockdown on Ambient Air Quality across Urban India, *Aerosol Air Qual. Res.*, 2020, **20**, 1759–1771.

3 A. Sikarwar and R. Rani, Assessing the Immediate Effect of Covid-19 Lockdown on Air Quality: A Case Study of Delhi, India, *J. Environ. Geogr.*, 2020, **13**, 27–33.

4 R. P. Singh and A. Chauhan, Impact of lockdown on air quality in India during COVID-19 pandemic, *Air Qual., Atmos. Health*, 2020, **13**, 921–928.

5 J. Zhang, K. Cui, Y.-F. Wang, J.-L. Wu, W.-S. Huang, S. Wan and K. Xu, Temporal Variations in the Air Quality Index and the Impact of the COVID-19 Event on Air Quality in Western China, *Aerosol Air Qual. Res.*, 2020, **20**, 1552–1568.

6 P. Wang, K. Chen, S. Zhu, P. Wang and H. Zhang, Severe air pollution events not avoided by reduced anthropogenic activities during COVID-19 outbreak, *Resour., Conserv. Recycl.*, 2020, **158**, 104814.

7 Y. Tan and T. Wang, What caused ozone pollution during the 2022 Shanghai lockdown? Insights from ground and satellite observations, *Atmos. Chem. Phys.*, 2022, **22**, 14455–14466.

8 M. C. Collivignarelli, A. Abbà, G. Bertanza, R. Pedrazzani, P. Ricciardi and M. Carnevale Miino, Lockdown for CoViD-2019 in Milan: What are the effects on air quality?, *Sci. Total Environ.*, 2020, **732**, 139280.

9 D. L. Goldberg, S. C. Anenberg, D. Griffin, C. A. McLinden, Z. Lu and D. G. Streets, Disentangling the Impact of the COVID-19 Lockdowns on Urban NO_2 From Natural Variability, *Geophys. Res. Lett.*, 2020, **47**, e2020GL089269.

10 S. Muhammad, X. Long and M. Salman, COVID-19 pandemic and environmental pollution: A blessing in disguise?, *Sci. Total Environ.*, 2020, **728**, 138820.

11 Z. Qu, D. J. Jacob, R. F. Silvern, V. Shah, P. C. Campbell, L. C. Valin and L. T. Murray, US COVID-19 Shutdown Demonstrates Importance of Background NO_2 in Inferring NO_x Emissions From Satellite NO_2 Observations, *Geophys. Res. Lett.*, 2021, **48**, e2021GL092783.

12 L. W. A. Chen, L.-C. Chien, Y. Li and G. Lin, Nonuniform impacts of COVID-19 lockdown on air quality over the United States, *Sci. Total Environ.*, 2020, **745**, 141105.

13 S. Mor, S. Kumar, T. Singh, S. Dogra, V. Pandey and K. Ravindra, Impact of COVID-19 lockdown on air quality in Chandigarh, India: Understanding the emission sources during controlled anthropogenic activities, *Chemosphere*, 2021, **263**, 127978.

14 M. Kganyago and L. Shikwambana, Did COVID-19 Lockdown Restrictions have an Impact on Biomass Burning Emissions in Sub-Saharan Africa?, *Aerosol Air Qual. Res.*, 2021, **21**, 200470.

15 B. Siciliano, G. Carvalho, C. M. da Silva and G. Arbilla, The Impact of COVID-19 Partial Lockdown on Primary Pollutant Concentrations in the Atmosphere of Rio de Janeiro and São Paulo Megacities (Brazil), *Bull. Environ. Contam. Toxicol.*, 2020, **105**, 2–8.

16 J. M. Baldasano, COVID-19 lockdown effects on air quality by NO_2 in the cities of Barcelona and Madrid (Spain), *Sci. Total Environ.*, 2020, **741**, 140353.

17 G. Varga, A. Csávics, J. Szeberényi and F. Gresina, Non-uniform tropospheric NO_2 level changes in European Union caused by governmental COVID-19 restrictions and geography, *City Environ. Interact.*, 2024, **22**, 100145.

18 Z. S. Venter, K. Aunan, S. Chowdhury and J. Lelieveld, COVID-19 lockdowns cause global air pollution declines, *Proc. Natl. Acad. Sci. U. S. A.*, 2020, **117**, 18984–18990.

19 K. Miyazaki, K. Bowman, T. Sekiya, M. Takigawa, J. L. Neu, K. Sudo, G. Osterman and H. Eskes, Global tropospheric ozone responses to reduced NO_x emissions linked to the COVID-19 worldwide lockdowns, *Sci. Adv.*, 2021, **7**, eabf7460.

20 T. Sekiya, K. Miyazaki, H. Eskes, K. Bowman, K. Sudo, Y. Kanaya and M. Takigawa, The worldwide COVID-19 lockdown impacts on global secondary inorganic aerosols and radiative budget, *Sci. Adv.*, 2023, **9**, eadh2688.

21 G. P. Chossière, H. Xu, Y. Dixit, S. Isaacs, S. D. Eastham, F. Allroggen, R. L. Speth and S. R. H. Barrett, Air pollution impacts of COVID-19–related containment measures, *Sci. Adv.*, 2021, **7**, eabe1178.

22 Z. Shi, C. Song, B. Liu, G. Lu, J. Xu, T. Van Vu, R. J. R. Elliott, W. Li, W. J. Bloss and R. M. Harrison, Abrupt but smaller than expected changes in surface air quality attributable to COVID-19 lockdowns, *Sci. Adv.*, 2021, **7**, eabd6696.

23 M. I. Mead, G. Okello, A. M. Mbandi and F. D. Pope, Spotlight on air pollution in Africa, *Nat. Geosci.*, 2023, **16**, 930–931.

24 L. Garcia, R. Johnson, A. Johnson, A. Abbas, R. Goel, L. Tatah, J. Damsere-Derry, E. Kyere-Gyeabour, M. Tainio, T. H. de Sá and J. Woodcock, Health impacts of changes in travel patterns in Greater Accra Metropolitan Area, Ghana, *Environ. Int.*, 2021, **155**, 106680.

25 P. D. M. C. Katoto, L. Byamungu, A. S. Brand, J. Mokaya, H. Strijdom, N. Goswami, P. De Boever, T. S. Nawrot and B. Nemery, Ambient air pollution and health in Sub-Saharan Africa: Current evidence, perspectives and a call to action, *Environ. Res.*, 2019, **173**, 174–188.

26 A. M. D. Navaratnam, H. Williams, S. J. Sharp, J. Woodcock and H. Khreis, Systematic review and meta-analysis on the impact of COVID-19 related restrictions on air quality in low- and middle-income countries, *Sci. Total Environ.*, 2024, **908**, 168110.

27 Health Effects Institute, *The State of Air Quality and Health Impacts in Africa. A Report from the State of Global Air Initiative*, Health Effects Institute, Boston, MA, 2022.

28 S. Fisher, D. C. Bellinger, M. L. Cropper, P. Kumar, A. Binagwaho, J. B. Koudenoukpo, Y. Park, G. Taghian and P. Landrigan, Air pollution and development in Africa: impacts on health, the economy, and human capital, *Lancet Planet. Health*, 2021, **5**, e681–e688.

29 K. Khomsi, H. Najmi, H. Amghar, Y. Chelhaoui and Z. Souhaili, COVID-19 national lockdown in morocco: Impacts on air quality and public health, *One Health*, 2021, **11**, 100200.

30 N. Yusuf, R. Said S, S. Tilmes and E. Gbobaniyi, Multi-year analysis of aerosol optical properties at various timescales using AERONET data in tropical West Africa, *J. Aerosol Sci.*, 2021, **151**, 105625.

31 V. Singh, S. Singh, A. Biswal, A. P. Kesarkar, S. Mor and K. Ravindra, Diurnal and temporal changes in air pollution during COVID-19 strict lockdown over different regions of India, *Environ. Pollut.*, 2020, **266**, 115368.

32 I. A. Fuwape, C. T. Okpalaonwuka and S. T. Ogunjo, Impact of COVID -19 pandemic lockdown on distribution of inorganic pollutants in selected cities of Nigeria, *Air Qual., Atmos. Health*, 2020, **14**, 149–155.

33 M. K. Mostafa, G. Gamal and A. Wafiq, The impact of COVID 19 on air pollution levels and other environmental indicators - A case study of Egypt, *J. Environ. Manage.*, 2021, **277**, 111496.

34 M. Abisha Meji, S. D. Milon and M. M, Effect of Covid-19 Induced Lockdown on Air Quality in Kampala, *i-Manager's J. Future Eng. Technol.*, 2020, **16**, 43–48.

35 K. Miyazaki, K. W. Bowman, K. Yumimoto, T. Walker and K. Sudo, Evaluation of a multi-model, multi-constituent assimilation framework for tropospheric chemical reanalysis, *Atmos. Chem. Phys.*, 2020, **20**, 931–967.

36 K. Miyazaki, K. Bowman, T. Sekiya, H. Eskes, F. Boersma, H. Worden, N. Livesey, V. H. Payne, K. Sudo, Y. Kanaya, M. Takigawa and K. Ogochi, Updated tropospheric chemistry reanalysis and emission estimates, TCR-2, for 2005–2018, *Earth Syst. Sci. Data*, 2020, **12**, 2223–2259.

37 T. Hale, N. Angrist, R. Goldszmidt, B. Kira, A. Petherick, T. Phillips, S. Webster, E. Cameron-Blake, L. Hallas, S. Majumdar and H. Tatlow, A global panel database of pandemic policies (Oxford COVID-19 Government Response Tracker), *Nat. Hum. Behav.*, 2021, **5**, 529–538.

38 K. Miyazaki, K. Bowman, T. Sekiya, Z. Jiang, X. Chen, H. Eskes, M. Ru, Y. Zhang and D. Shindell, Air Quality Response in China Linked to the 2019 Novel Coronavirus (COVID-19) Lockdown, *Geophys. Res. Lett.*, 2020, **47**, e2020GL089252.

39 J. W. Kaiser, A. Heil, M. O. Andreae, A. Benedetti, N. Chubarova, L. Jones, J. J. Morcrette, M. Razinger, M. G. Schultz, M. Suttie and G. R. van der Werf, Biomass burning emissions estimated with a global fire assimilation system based on observed fire radiative power, *Biogeosciences*, 2012, **9**, 527–554.

40 G. Janssens-Maenhout, M. Crippa, D. Guizzardi, F. Dentener, M. Muntean, G. Pouliot, T. Keating, Q. Zhang, J. Kurokawa, R. Wankmüller, H. Denier van der Gon, J. J. P. Kuenen, Z. Klimont, G. Frost, S. Darras, B. Koffi and M. Li, HTAP_v2.2: a mosaic of regional and global emission grid maps for 2008 and 2010 to study hemispheric transport of air pollution, *Atmos. Chem. Phys.*, 2015, **15**, 11411–11432.

41 J. J. Yienger and H. Levy II, Empirical model of global soil-biogenic NO_x emissions, *J. Geophys. Res.:Atmos.*, 1995, **100**, 11447–11464.

42 C. Price and D. Rind, A simple lightning parameterization for calculating global lightning distributions, *J. Geophys. Res.:Atmos.*, 1992, **97**, 9919–9933.

43 J. H. G. M. van Geffen, H. J. Eskes, K. F. Boersma, J. D. Maasakkers, and J. P. Veefkind, *TROPOMI ATBD of the Total and Tropospheric NO_2 Data Products*, 2024.

44 K. Chen, M. Wang, C. Huang, P. L. Kinney and P. T. Anastas, Air pollution reduction and mortality benefit during the COVID-19 outbreak in China, *Lancet Planet. Health*, 2020, **4**, e210–e212.

45 H. Li, B. Zheng, P. Ciais, K. F. Boersma, T. C. V. W. Riess, R. V. Martin, G. Broquet, R. van der A, H. Li, C. Hong, Y. Lei, Y. Kong, Q. Zhang and K. He, Satellite reveals a steep decline in China's CO_2 emissions in early 2022, *Sci. Adv.*, 2023, **9**, eadg7429.

46 Y. Ma, F. Nobile, A. Marb, R. Dubrow, P. L. Kinney, A. Peters, M. Stafoggia, S. Breitner and K. Chen, Air pollution changes due to COVID-19 lockdowns and attributable mortality changes in four countries, *Environ. Inter.*, 2024, **187**, 108668.

47 Y. Zhang, B. Zhao, Y. Jiang, J. Xing, S. K. Sahu, H. Zheng, D. Ding, S. Cao, L. Han, C. Yan, X. Duan, J. Hu, S. Wang and J. Hao, Non-negligible contributions to human health from increased household air pollution exposure during the COVID-19 lockdown in China, *Environ. Int.*, 2022, **158**, 106918.

48 H. Guo, Y. Zhu, Y. Qian and M. Wu, Confidence interval estimation for the difference of censored zero-inflated gamma distributions, *Sci. Rep.*, 2024, **14**, 29435.

49 L. Zhang, F. Huettmann, S. Liu, P. Sun, Z. Yu, X. Zhang and C. Mi, Classification and regression with random forests as a standard method for presence-only data SDMs: A future conservation example using China tree species, *Ecol. Inform.*, 2019, **52**, 46–56.

50 F. Shen, M. I. Hegglin and Y. Yuan, Impact of weather patterns and meteorological factors on $PM_{2.5}$ and O_3 responses to the COVID-19 lockdown in China, *Atmos. Chem. Phys.*, 2024, **24**, 6539–6553.

51 W. E. Cahyono, A. Anwar, D. Gusnita, F. Rahmatia, H. Santoso, P. Y. Kombara, S. Sumaryati, W. Setyawati, W. J. Sari, Y. Susilowati, T. Kartika, A. Y. Putra and N. F. Romadona, in *Urban Commons, Future Smart Cities and Sustainability*, ed. U. Chatterjee, N. Bandyopadhyay, M. D. Setiawati and S. Sarkar, Springer International Publishing, Cham, 2023, pp. 957–979.

52 M. Xiang, C. Xiao, Z. Feng and Q. Ma, Global distribution, trends and types of active fire occurrences, *Sci. Total Environ.*, 2023, **902**, 166456.

53 L. Shikwambana, Long-term observation of global black carbon, organic carbon and smoke using CALIPSO and MERRA-2 data, *Remote Sens. Lett.*, 2019, **10**, 373–380.

54 L. Bremond, J. C. Aleman, C. Favier, O. Blarquez, D. Colombaroli, S. E. Connor, C. E. Cordova, C. Courtney-Mustaphi, A. N. Dabengwa, G. Gil-Romera, W. D. Gosling, T. Hamilton, V. Montade, A. H. I. Razafimanantsoa, M. J. Power, E. Razanatsoa, I. Yabi and B. Vannière, Past fire dynamics in sub-Saharan Africa during the last 25,000 years: Climate change and increasing human impacts, *Quat. Int.*, 2024, **711**, 49–58.

55 L. Zhang and Z. Zhang, Wildfires and Climate Change as Key Drivers of Forest Carbon Flux Variations in Africa over the Past Two Decades, *Fire*, 2025, **8**, 333.

56 E. E. Ukpebor, J. E. Ukpebor, F. Eromomene, J. I. Odiase and D. Okoro, Spatial and diurnal variations of Carbon monoxide (CO) pollution from motor vehicles in an Urban centre, *Pol. J. Environ. Stud.*, 2010, **19**, 817–823.

57 W. Hua, S. Lou, X. Huang, L. Xue, K. Ding, Z. Wang and A. Ding, Diagnosing uncertainties in global biomass burning emission inventories and their impact on modeled air pollutants, *Atmos. Chem. Phys.*, 2024, **24**, 6787–6807.

58 O. G. Fawole, N. Yusuf, L. A. Sunmonu, A. Obafaye, D. K. Audu, L. Onuorah, C. F. Olusegun, A. Deme and H. Senghor, Impacts of COVID-19 Restrictions on Regional and Local Air Quality Across Selected West African Cities, *GeoHealth*, 2022, **6**, e2022GH000597.

59 J. E. Hickman, N. Andela, K. Tsigaridis, C. Galy-Lacaux, M. Ossohou, E. Dammers, M. Van Damme, L. Clarisse and S. E. Bauer, Continental and Ecoregion-Specific Drivers of Atmospheric NO_2 and NH_3 Seasonality Over Africa Revealed by Satellite Observations, *Global Biogeochem. Cycles*, 2021, **35**, e2020GB006916.

60 S. Dahiya, A. Anhäuser, A. Farrow, H. Thieriot, A. Chanchal and L. Myllyvirta, *Ranking the World's Sulfur Dioxide (SO_2) Hotspots: 2019-2020*, Center for Research on Energy and Clean Air & Greenpeace India, Delhi, 2020.

61 K. E. Agbo, C. Walgraeve, J. I. Eze, P. E. Ugwoke, P. O. Ukoha and H. Van Langenhove, A review on ambient and indoor air pollution status in Africa, *Atmos. Pollut. Res.*, 2021, **12**, 243–260.

62 N. R. Matandirotya, S. D. Moletsane, E. Matandirotya and R. P. Burger, State of ambient air quality in a low-income urban settlement of South Africa, *Sci. Afr.*, 2022, **16**, e01201.

63 J. A. Adesina, S. J. Piketh, R. P. Burger and G. Mkhatshwa, Assessment of criteria pollutants contributions from coal-fired plants and domestic solid fuel combustion at the South African industrial highveld, *Clean. Eng. Technol.*, 2022, **6**, 100358.

64 S. P. Hersey, R. M. Garland, E. Crosbie, T. Shingler, A. Sorooshian, S. Piketh and R. Burger, An overview of regional and local characteristics of aerosols in South Africa using satellite, ground, and modeling data, *Atmos. Chem. Phys.*, 2015, **15**, 4259–4278.

65 P. Wetchayont and I. Levy, Investigation on the Impacts of COVID-19 Lockdown and Influencing Factors on Air Quality in Greater Bangkok, Thailand, *Adv. Meteorol.*, 2021, **2021**, 1–11.

66 B. Kotan and A. Erener, Seasonal analysis and mapping of air pollution (PM_{10} and SO_2) during Covid-19 lockdown in Kocaeli (Turkiye), *Int. J. Eng. Geosci.*, 2023, **8**, 173–187.

67 S. Mahato, S. Pal and K. G. Ghosh, Effect of lockdown amid COVID-19 pandemic on air quality of the megacity Delhi, India, *Sci. Total Environ.*, 2020, **730**, 139086.

68 F. Qayyum, S. Tariq, H. Nawaz, Z. ul-Haq, U. Mehmood and Z. B. Babar, Variation of air pollutants during COVID-19 lockdown phases in the mega-city of Lahore (Pakistan); Insights into meteorological parameters and atmospheric chemistry, *Acta Geophys.*, 2024, **72**, 2083–2096.

69 C. M. Nussbaumer, H. Fischer, J. Lelieveld and A. Pozzer, What controls ozone sensitivity in the upper tropical troposphere?, *Atmos. Chem. Phys.*, 2023, **23**, 12651–12669.

70 Y. Choi, H. Kim, D. Tong and P. Lee, Summertime weekly cycles of observed and modeled NO_x and O_3 concentrations as a function of satellite-derived ozone production sensitivity and land use types over the Continental United States, *Atmos. Chem. Phys.*, 2012, **12**, 6291–6307.

71 B. N. Duncan, Y. Yoshida, J. R. Olson, S. Sillman, R. V. Martin, L. Lamsal, Y. Hu, K. E. Pickering, C. Retscher, D. J. Allen and J. H. Crawford, Application of OMI observations to a space-based indicator of NO_x and VOC controls on surface ozone formation, *Atmos. Environ.*, 2010, **44**, 2213–2223.

72 T. L. Laban, P. G. van Zyl, J. P. Beukes, V. Vakkari, K. Jaars, N. Borduas-Dedekind, M. Josipovic, A. M. Thompson, M. Kulmala and L. Laakso, Seasonal influences on surface ozone variability in continental South Africa and implications for air quality, *Atmos. Chem. Phys.*, 2018, **18**, 15491–15514.

73 N. Wang, X. Lyu, X. Deng, X. Huang, F. Jiang and A. Ding, Aggravating O_3 pollution due to NO_x emission control in eastern China, *Sci. Total Environ.*, 2019, **677**, 732–744.

74 N. Borduas-Dedekind, M. Naidoo, B. Zhu, J. Geddes and R. M. Garland, Tropospheric ozone (O_3) pollution in Johannesburg, South Africa: Exceedances, diurnal cycles, seasonality, O_x chemistry and O_3 production rates, *Clean Air J.*, 2023, **33**, 1–16.

75 V. Vakkari, J. P. Beukes, M. Josipovic and P. G. van Zyl, Observations of ozone formation in southern African savanna and grassland fire plumes, *Atmos. Environ.*, 2020, **223**, 117256.

76 Y. Liu, T. Wang, T. Stavrakou, N. Elguindi, T. Doumbia, C. Granier, I. Bouarar, B. Gaubert and G. P. Brasseur, Diverse response of surface ozone to COVID-19 lockdown in China, *Sci. Total Environ.*, 2021, **789**, 147739.

77 M. A. Zoran, R. S. Savastru, D. M. Savastru and M. N. Tautan, Assessing the relationship between ground levels of ozone (O_3) and nitrogen dioxide (NO_2) with coronavirus (COVID-19) in Milan, Italy, *Sci. Total Environ.*, 2020, **740**, 140005.

78 R. Tang, X. Huang, D. Zhou, H. Wang, J. Xu and A. Ding, Global air quality change during the COVID-19 pandemic: Regionally different ozone pollution responses COVID-19, *Atmos. Oceanic Sci. Lett.*, 2021, **14**, 100015.

79 S. Gao, D. A. Hegg, P. V. Hobbs, T. W. Kirchstetter, B. I. Magi and M. Sadilek, Water-soluble organic components in aerosols associated with savanna fires in southern Africa: Identification, evolution, and distribution, *J. Geophys. Res.:Atmos.*, 2003, **108**, 8491.

80 L. J. S. Borlaza, V. D. Ngoc Thuy, S. Grange, S. Socquet, E. Moussu, G. Mary, O. Favez, C. Hueglin, J.-L. Jaffrezo and G. Uzu, Impact of COVID-19 lockdown on particulate matter oxidative potential at urban background versus traffic sites, *Environ. Sci.: Atmos.*, 2023, **3**, 942–953.

81 T. O. Etchie, A. T. Etchie, A. Jauro, R. T. Pinker and N. Swaminathan, Season, not lockdown, improved air quality during COVID-19 State of Emergency in Nigeria, *Sci. Total Environ.*, 2021, **768**, 145187.

82 T. Le, Y. Wang, L. Liu, J. Yang, Y. L. Yung, G. Li and J. H. Seinfeld, Unexpected air pollution with marked emission reductions during the COVID-19 outbreak in China, *Science*, 2020, **369**, 702–706.

83 M. Li, T. Wang, M. Xie, S. Li, B. Zhuang, Q. Fu, M. Zhao, H. Wu, J. Liu, E. Saikawa and K. Liao, Drivers for the poor air quality conditions in North China Plain during the COVID-19 outbreak, *Atmos. Environ.*, 2021, **246**, 118103.

84 L. A. Chen, L. C. Chien, Y. Li and G. Lin, Nonuniform impacts of COVID-19 lockdown on air quality over the United States, *Sci. Total Environ.*, 2020, **745**, 141105.

85 N. Vig, K. Ravindra and S. Mor, Environmental impacts of Indian coal thermal power plants and associated human health risk to the nearby residential communities: A potential review, *Chemosphere*, 2023, **341**, 140103.

86 N. Huneeus, M. Schulz, Y. Balkanski, J. Griesfeller, J. Prospero, S. Kinne, S. Bauer, O. Boucher, M. Chin, F. Dentener, T. Diehl, R. Easter, D. Fillmore, S. Ghan, P. Ginoux, A. Grini, L. Horowitz, D. Koch, M. C. Krol, W. Landing, X. Liu, N. Mahowald, R. Miller, J. J. Morcrette, G. Myhre, J. Penner, J. Perlwitz, P. Stier, T. Takemura and C. S. Zender, Global dust model intercomparison in AeroCom phase I, *Atmos. Chem. Phys.*, 2011, **11**, 7781–7816.

87 R. W. Burgess and M. I. Oyola-Merced, *Radiative Examination of Developing African Easterly Waves and Saharan Dust Interactions: Comparative Insights from Reanalysis and NASA Airborne Observations*, EGUsphere, 2024, pp. 1–26.

88 V. Singh, A. Biswal, A. P. Kesarkar, S. Mor and K. Ravindra, High resolution vehicular PM_{10} emissions over megacity Delhi: Relative contributions of exhaust and non-exhaust sources, *Sci. Total Environ.*, 2020, **699**, 134273.

89 C. Lou, H. Liu, Y. Li, Y. Peng, J. Wang and L. Dai, Relationships of relative humidity with $PM_{2.5}$ and PM_{10} in the Yangtze River Delta, China, *Environ. Monit. Assess.*, 2017, **189**, 582.

90 A. D. Bhanarkar, S. K. Goyal, R. Sivacoumar and C. V. Chalapati Rao, Assessment of contribution of SO_2 and NO_2 from different sources in Jamshedpur region, India, *Atmos. Environ.*, 2005, **39**, 7745–7760.

91 D. Fattorini and F. Regoli, Role of the chronic air pollution levels in the Covid-19 outbreak risk in Italy, *Environ. Pollut.*, 2020, **264**, 114732.

92 J. N. D. Gordon, K. R. Bilsback, M. N. Fiddler, R. P. Pokhrel, E. V. Fischer, J. R. Pierce and S. Bililign, The Effects of Trash, Residential Biofuel, and Open Biomass Burning Emissions on Local and Transported $PM_{2.5}$ and Its Attributed Mortality in Africa, *GeoHealth*, 2023, **7**, e2022GH000673.

93 Q. Ma, Y. Liu and H. He, Synergistic Effect between NO_2 and SO_2 in Their Adsorption and Reaction on γ-Alumina, *J. Phys. Chem. A*, 2008, **112**, 6630–6635.

94 Q. Wang, X. Dong, J. S. Fu, J. Xu, C. Deng, Y. Jiang, Q. Fu, Y. Lin, K. Huang and G. Zhuang, Environmentally dependent dust chemistry of a super Asian dust storm in March 2010: observation and simulation, *Atmos. Chem. Phys.*, 2018, **18**, 3505–3521.

95 S. P. Simelane and K. E. Langerman, The sensitivity of health impact assessments of $PM_{2.5}$ from South African coal-fired power stations, *Air Qual., Atmos. Health*, 2024, **17**, 325–340.

